

Entropy stable discontinuous Galerkin methods for ten-moment Gaussian closure equations

Biswarup Biswas[†], Harish Kumar[†], and Anshu Yadav[†]

[†]Department of Mathematics, Indian Institute of Technology Delhi, New Delhi, India-110016

Abstract

In this article, we propose high order discontinuous Galerkin entropy stable schemes for ten-moment Gaussian closure equations, which is based on the suitable quadrature rules (see [8]). The key components of the proposed method are the use of an entropy conservative numerical flux [31] in each cell and a suitable entropy stable numerical flux at the cell edges. This is then used in the entropy stable DG framework of [8] to obtain entropy stability of the semi-discrete scheme. We also extend these schemes to a source term that models plasma laser interaction. For the time discretization, we use strong stability preserving schemes. The proposed schemes are then tested on several test cases to demonstrate stability, accuracy, and robustness.

Keywords— Discontinuous Galerkin scheme, entropy stability, high-order accurate scheme, balance laws

1 Introduction

In several fluid and plasma flow applications assumptions of the *local thermodynamic equilibrium* do not hold (see [14, 29, 5, 28, 19, 25]). Due to this, the simulations of such flows using the scalar description of the pressure (used most commonly in Euler equations of compressible fluid flows) is not accurate and instead a tensorial pressure (and hence temperature) is needed. One such model is ten-moment Gaussian closure equations (see [1, 2, 26, 31, 24, 25, 21, 22]). It is one of the simplest fluid model which consider pressure as tensor.

The system of the ten-moment Gaussian closure equations is a nonlinear system of hyperbolic conservation laws [22]. So, the solutions of the corresponding Cauchy problem may contain discontinuities, even with smooth initial data. Hence, weak solutions are considered. Furthermore, to rule out the physically irrelevant solutions, an additional criterion in the form of entropy stability is imposed. Due to the presence of the nonlinear flux, the theoretical existence of the solutions is highly unlikely for most of the problems. Hence computational methods are used for most of the applications. Numerical methods for hyperbolic PDEs are often based on the finite volume methods [20], where higher-order accuracy is achieved using TVD, ENO, or WENO based reconstruction process. Another prevalent method is discontinuous Galerkin (DG) schemes, first developed by Reed and Hill in [30] in the context of neutron transport problems. They were generalized for the time-dependent hyperbolic problems in [7] and improved in [10, 11]. These schemes show significant improvement in accuracy in comparison to the finite volume schemes of the equivalent order.

One of the most important theoretical estimates for the solutions of hyperbolic conservation laws is entropy stability. For the discrete solutions to be physically relevant, we need to ensure that they satisfy a discrete entropy inequality. However, this is highly nontrivial for the higher-order schemes. In [15], authors have developed entropy stable higher-order numerical schemes. These are further extended to TVD [13, 3] and WENO schemes [16]. Entropy stable DG schemes were developed for Shallow water equations in [17]. More recently, a general framework of constructing entropy stable DG scheme for hyperbolic conservation laws is proposed by Chen and Shu in [8] and applied to Euler's equations. This framework is also applied to several other interesting hyperbolic conservation laws [23, 12, 4].

For the Ten-Moment equations, several numerical schemes have been developed. In [1, 2] Berthon has developed first-order entropy stable and first-order positivity preserving schemes. The positivity preserving schemes are then extended to higher-order finite volume, DG, and WENO schemes by Meena et al. in [26, 25, 27]. Furthermore, in [24], authors have proposed a well-balanced scheme for a potential type source terms. For the entropy stability of schemes, authors in [31] developed higher-order entropy stable finite difference schemes.

In this work, we design higher-order entropy stable DG schemes for ten-moment Gaussian closure equations. We proceed as follows:

- Following [31], we first present the entropy framework for the ten-moment Gaussian closure equations.
- We then discretize the equations using the suitable quadrature rules presented in [8].
- To achieve the entropy stability of the scheme, we use entropy conservative numerical flux from [31] and a suitable entropy stable flux at the cell edges.
- The scheme is then extended to include the potential type source terms.

The rest of the article is organized as follows: In Section 2, we present the ten-moment Gaussian closure equations and related entropy framework. In Section 3 we presents the one-dimensional scheme. We prove the accuracy, consistency, and the entropy stability of the schemes. These schemes are then extended to the two-dimensional case in Section 4. Extensive numerical results for one and two-dimensional test cases are presented in Section 5.

2 Ten-moment Gaussian closure equations

Following [2, 31, 26], we consider the following two-dimensional ten-moment Gaussian closure model with source terms:

$$\partial_t \mathbf{u} + \partial_x \mathbf{f}(\mathbf{u}) + \partial_y \mathbf{g}(\mathbf{u}) = \mathbf{s}^x(\mathbf{u}) + \mathbf{s}^y(\mathbf{u}), \quad (1)$$

where $\mathbf{u} = (\rho, \rho \vec{v}, \mathbf{E})^T$ is the vector of the conservative variables. Here ρ is the fluid density, vector $\vec{v} = (v^x, v^y)^T$ is the fluid velocity and symmetric tensor $\mathbf{E} = (E^{xx}, E^{xy}, E^{yy})^T$ is the energy tensor. The fluxes \mathbf{f} and \mathbf{g} are given by,

$$\mathbf{f}(\mathbf{u}) = \begin{pmatrix} \rho v^x \\ \rho (v^x)^2 + p^{xx} \\ \rho v^x v^y + p^{xy} \\ \rho v^{x3} + 3v^x p^{xx} \\ \rho (v^x)^2 v^y + 2v^x p^{xy} + v^y p^{xx} \\ \rho v^x (v^y)^2 + v^x p^{yy} + 2v^y p^{xy} \end{pmatrix}, \text{ and } \mathbf{g}(\mathbf{u}) = \begin{pmatrix} \rho v^y \\ \rho v^x v^y + p^{xy} \\ \rho (v^y)^2 + p^{yy} \\ \rho v^y (v^x)^2 + v^y p^{xx} + 2v^x p^{xy} \\ \rho (v^y)^2 v^x + 2v^y p^{xy} + v^x p^{yy} \\ \rho (v^y)^3 + 3v^y p^{yy} \end{pmatrix}.$$

The source terms in (1) are given by,

$$\mathbf{s}_x(\mathbf{u}) = \begin{pmatrix} 0 \\ -\frac{1}{2}\rho\partial_x W \\ 0 \\ -\rho v^x \partial_x W \\ -\frac{1}{2}\rho v^y \partial_x W \\ 0 \end{pmatrix}, \text{ and } \mathbf{s}_y(\mathbf{u}) = \begin{pmatrix} 0 \\ 0 \\ -\frac{1}{2}\rho\partial_y W \\ 0 \\ -\frac{1}{2}\rho v^x \partial_y W \\ -\rho v^y \partial_y W \end{pmatrix},$$

where $W(x, y, t)$ is the given function, which models electron quiver energy in the laser. The system (1) is closed by the using equation of state expression,

$$\mathbf{E} = \rho \vec{v} \otimes \vec{v} + \mathbf{p}, \quad (2)$$

where $\mathbf{p} = (p^{xx}, p^{xy}, p^{yy})^T$ is the symmetric pressure tensor. For the solutions to be physically admissible, we need density and symmetric pressure tensor to be positive. Hence, we consider the following set Ω of physically admissible weak solutions:

$$\Omega = \{ \mathbf{u} \in \mathbb{R}^6 \mid \rho > 0, \mathbf{x}^T \mathbf{p} \mathbf{x} > 0, \forall \mathbf{x} \in \mathbb{R}^2 \text{ with } \mathbf{x} \neq \mathbf{0} \}. \quad (3)$$

For solutions, $\mathbf{u} \in \Omega$, we have the following results from [22, 1]:

Lemma 2.1. *The system (1) is hyperbolic for $\mathbf{u} \in \Omega$. Furthermore, the eigenvalues are given as,*

$$\vec{v} \cdot \mathbf{n}, \vec{v} \cdot \mathbf{n} \pm \sqrt{\frac{3(\mathbf{p} \cdot \mathbf{n}) \cdot \mathbf{n}}{\rho}}, \vec{v} \cdot \mathbf{n} \pm \sqrt{\frac{(\mathbf{p} \cdot \mathbf{n}) \cdot \mathbf{n}}{\rho}},$$

along the unitary vector \mathbf{n} . The multiplicity of the eigenvalue $\vec{v} \cdot \mathbf{n}$ is two and multiplicity of all other eigenvalues have is one. In addition, the eigenvalue $\vec{v} \cdot \mathbf{n}$ is associated to a linearly degenerate field. The eigenvalues $\vec{v} \cdot \mathbf{n} \pm \sqrt{\frac{3(\mathbf{p} \cdot \mathbf{n}) \cdot \mathbf{n}}{\rho}}$ are associated to a genuinely nonlinear field while eigenvalues $\vec{v} \cdot \mathbf{n} \pm \sqrt{\frac{(\mathbf{p} \cdot \mathbf{n}) \cdot \mathbf{n}}{\rho}}$ are associated to a linearly degenerate field.

In order to choose *physically relevant* solutions, following [2, 31], we will now describe the entropy framework. Let us define the following:

Definition 2.1. *A convex function \mathcal{U} is said to be an entropy function for conservation laws (1) if there exist smooth functions \mathcal{F} and \mathcal{G} such that*

$$\mathcal{F}' = \mathcal{U}'(\mathbf{u}) \mathbf{f}'(\mathbf{u}), \quad \mathcal{G}' = \mathcal{U}'(\mathbf{u}) \mathbf{g}'(\mathbf{u}). \quad (4)$$

For the ten-moment Gaussian closure equations (1), following [31], we consider entropy \mathcal{U} and the entropy fluxes as follows:

$$\mathcal{U} = -\rho s, \quad \mathcal{F} = \rho v^x s, \quad \mathcal{G} = \rho v^y s, \quad (5)$$

where $s = \ln \left(\frac{\det(\mathbf{p})}{\rho^4} \right)$. For the smooth solutions, we have the following equality (see [31]):

$$\frac{\partial \mathcal{U}}{\partial t} + \frac{\partial \mathcal{F}}{\partial x} + \frac{\partial \mathcal{G}}{\partial y} = 0, \quad (6)$$

which for non-smooth weak solutions become *entropy inequality*:

$$\frac{\partial \mathcal{U}}{\partial t} + \frac{\partial \mathcal{F}}{\partial x} + \frac{\partial \mathcal{G}}{\partial y} \leq 0. \quad (7)$$

Using entropy \mathcal{U} , we define entropy variable $\mathbf{v} = \partial_{\mathbf{u}}\mathcal{U}$. A lengthy calculation results in the following expression for \mathbf{v} :

$$\mathbf{v} = \partial_{\mathbf{u}}\mathcal{U} = \begin{pmatrix} 4 - s - \frac{\rho}{\det(\mathbf{p})} \left(p^{xx} (v^y)^2 + p^{yy} (v^x)^2 - 2p^{xy} v^x v^y \right) \\ \frac{2\rho v^y}{\det(\mathbf{p})} \\ \frac{\det(\mathbf{p})}{\rho p^{yy}} \\ -\frac{\det(\mathbf{p})}{2\rho p^{xy}} \\ \frac{\det(\mathbf{p})}{\rho p^{xx}} \\ -\frac{\det(\mathbf{p})}{\det(\mathbf{p})} \end{pmatrix}$$

In the following sections, we aim to design DG schemes which satisfy (7) at semi-discrete level.

3 Entropy Stable DG Schemes: One dimensional scheme

To simplify the presentation, we will first present the numerical schemes for the one-dimensional model:

$$\partial_t \mathbf{u} + \partial_x \mathbf{f}(\mathbf{u}) = \mathbf{s}^x(\mathbf{u}). \quad (8)$$

We discretize the x -spatial domain into N elements $I_i = [x_{i-\frac{1}{2}}, x_{i+\frac{1}{2}}]$ ($1 \leq i \leq N$). Then we seek a solution,

$$\mathbf{w}_h \in \mathbf{V}_h^k := \left\{ \mathbf{v}_h : \mathbf{v}_h|_{I_i} \in [\mathcal{P}^k(I_i)]^6, 1 \leq i \leq N \right\},$$

such that for all $\mathbf{v}_h \in \mathbf{V}_h^k$ and for all $1 \leq i \leq N$,

$$\begin{aligned} \int_{I_i} \frac{\partial \mathbf{w}_h^T}{\partial t} \mathbf{v}_h dx - \int_{I_i} \mathbf{f}(\mathbf{w}_h)^T \frac{d\mathbf{v}_h}{dx} dx \\ + \hat{\mathbf{f}}_{i+1/2}^T \mathbf{v}_h(x_{i+1/2}^-) - \hat{\mathbf{f}}_{i-1/2}^T \mathbf{v}_h(x_{i-1/2}^+) = \int_{I_i} \mathbf{s}^x(\mathbf{w}_h)^T \mathbf{v}_h dx. \end{aligned} \quad (9)$$

Here, $\hat{\mathbf{f}}_{i+1/2}$ is a numerical flux depends on the numerical solutions at element interface, that is, $\hat{\mathbf{f}}_{i+1/2} = \hat{\mathbf{f}}(\mathbf{w}_h(x_{i+1/2}^-), \mathbf{w}_h(x_{i+1/2}^+))$. We intend to apply Gauss-Lobatto quadrature to the integrals in (9). To present the quadrature rules, we first consider the scalar case. This can be easily extended to (9). Now applying the change of variable

$$x = \frac{x_{i+1/2} + x_{i-1/2}}{2} + \frac{1}{2}\xi\Delta x_i,$$

we have the following

$$\begin{aligned} \frac{\Delta x_i}{2} \int_I \frac{\partial w_h}{\partial t} v_h d\xi - \int_I f(w_h) \frac{dv_h}{d\xi} d\xi \\ + \hat{f}_{i+1/2} v_h(1) - \hat{f}_{i-1/2} v_h(-1) = \frac{\Delta x_i}{2} \int_I s_x(w_h) v_h d\xi, \end{aligned}$$

with $I = [-1, 1]$. Given the GaussLobatto quadrature points,

$$-1 = \xi_0 < \xi_1 < \xi_2 \dots < \xi_k = 1,$$

and the corresponding weights ω_j , $0 \leq j \leq k$, we consider the following nodal basis,

$$L_j(\xi) = \prod_{l=0, l \neq j}^N \frac{\xi - \xi_l}{\xi_j - \xi_l}.$$

Then w_h is given by, $w_h = \sum_{j=0}^k u_j^i L_j(\xi)$. Furthermore, we approximate $f(w_h)$ and $s_x(w_h)$ as,

$$f(w_h) \approx f_h(\xi) := \sum_{j=0}^k f(u_j^i) L_j(\xi), \quad s_x(w_h) \approx s_{x,h}(\xi) := \sum_{j=0}^k s_x(u_j^i) L_j(\xi). \quad (10)$$

Finally, choosing the test function $v_h = L_j$, we have,

$$\frac{\Delta x_i}{2} \frac{d}{dt} \langle w_h, L_j \rangle_h - \langle f_h, L_j' \rangle_h + \hat{f}_{i+1/2} L_j(1) - \hat{f}_{i-1/2} L_j(-1) = \frac{\Delta x_i}{2} \langle s_{x,h}, L_j \rangle_h. \quad (11)$$

where we use the inner product notation,

$$\langle u, v \rangle := \int_I u v d\xi, \quad \langle u, v \rangle_h := \sum_{j=0}^k \omega_j u(\xi_j) v(\xi_j).$$

By using 10, Equation (11) can be further written as,

$$\frac{\Delta x_i}{2} \sum_{l=0}^k \frac{d u_l^i}{dt} \langle L_l, L_j \rangle_h - \sum_{l=0}^k f_l^i \langle L_l, L_j' \rangle_h + \hat{f}_{i+1/2} L_j(1) - \hat{f}_{i-1/2} L_j(-1) = \frac{\Delta x_i}{2} \sum_{l=0}^k s_x(u_l^i) \langle L_l, L_j \rangle_h. \quad (12)$$

For a compact form of the scheme, let us define the matrices D , M and S as,

$$\begin{cases} D_{jl} = L_l'(\xi_j), \\ M_{jl} = \langle L_j, L_l \rangle_h = \omega_j \delta_{jl}, \\ S_{jl} = \langle L_j, L_l' \rangle_h = \langle L_j, L_l' \rangle. \end{cases}$$

Also, define the boundary matrix as,

$$B = \text{diag}[\tau_0, \tau_1, \dots, \tau_k], \quad \text{where } \tau_j := \begin{cases} -1 & j = 0 \\ 0 & 1 \leq j \leq k-1 \\ 1 & j = k \end{cases}. \quad (13)$$

These matrices are also known as summation-by-parts (SBP) matrices and has the following properties:

1. SBP property ([6]):

$$\begin{cases} S = MD, \\ MD + D^T M = S + S^T = B. \end{cases} \quad (14)$$

2. For $0 \leq j \leq k$ we have (see [8]),

$$\sum_{l=0}^k D_{jl} = \sum_{l=0}^k S_{jl} = 0, \quad \sum_{l=0}^k S_{lj} = \tau_j. \quad (15)$$

With the SBP matrices defined above, (12) can be simplified as,

$$\frac{\Delta x_i}{2} M \frac{du^i}{dt} - S^T f^i + B \hat{f}^i = \frac{\Delta x_i}{2} M s_x^i. \quad (16)$$

where, we have used the following notations,

$$\begin{aligned} u^i &= [u_0^i, \dots, u_k^i]^T \\ f^i &= [f_0^i, \dots, f_k^i]^T \\ s_x^i &= [s_x(u_0^i), \dots, s_x(u_k^i)]^T, \\ \hat{f}^i &= [f_{i-1/2}, 0, \dots, 0, f_{i+1/2}]^T. \end{aligned}$$

The scheme (16) can now be written in the following form,

$$\frac{du^i}{dt} + \frac{2}{\Delta x_i} D f^i = \frac{2}{\Delta x_i} M^{-1} B (f^i - \hat{f}^i) + s_x^i. \quad (17)$$

For a single element, this scheme can be written as (ignoring the element index i),

$$\frac{du_j}{dt} + \frac{2}{\Delta x} \sum_{l=0}^k D_{jl} f_l = \frac{2}{\Delta x} \frac{\tau_j}{\omega_j} (f_j - \hat{f}_j) + (s_x)_j. \quad (18)$$

A similar analysis works for the system case (see [8]), and without loss of generality, the scheme (18) can be extended to (8) as,

$$\frac{d\mathbf{u}_j}{dt} + \frac{2}{\Delta x} \sum_{l=0}^k D_{jl} \mathbf{f}_l = \frac{2}{\Delta x} \frac{\tau_j}{\omega_j} (\mathbf{f}_j - \hat{\mathbf{f}}_j) + (\mathbf{s}_x)_j. \quad (19)$$

In general, we do not have an entropy stability proof of the scheme (19). However, a modification to the scheme (19) provides an entropy estimation. First, let us consider the following definitions:

Definition 3.1. A two point symmetric, consistent numerical flux \mathbf{f}^* is said to be entropy conservative flux for an entropy function \mathcal{U} if

$$(\mathbf{v}_R - \mathbf{v}_L)^T \mathbf{f}^*(\mathbf{u}_R, \mathbf{u}_L) = \psi_R - \psi_L, \quad (20)$$

where $\mathbf{v} = \mathcal{U}'(\mathbf{u})$ is known as entropy variable, and $\psi = \mathbf{v}^T \cdot \mathbf{f} - \mathcal{F}$ is the entropy potential. L and R in suffix denote the left and right state.

Definition 3.2. A two-point symmetric, consistent numerical flux \mathbf{f} is said to be entropy stable flux for the entropy function \mathcal{U} if

$$(\mathbf{v}_R - \mathbf{v}_L)^T \mathbf{f}(\mathbf{u}_R, \mathbf{u}_L) \leq \psi_R - \psi_L. \quad (21)$$

We modify (19) as,

$$\frac{d\mathbf{u}_j}{dt} + \frac{4}{\Delta x} \sum_{l=0}^k D_{jl} \mathbf{f}^*(\mathbf{u}_j, \mathbf{u}_l) = \frac{2}{\Delta x} \frac{\tau_j}{\omega_j} (\mathbf{f}_j - \hat{\mathbf{f}}_j) + (\mathbf{s}_x)_j. \quad (22)$$

where \mathbf{f}^* is taken to be entropy conservative. Then we have the following result.

Theorem 3.1 ([8]). If $\mathbf{f}^*(\mathbf{u}_j, \mathbf{u}_l)$ is consistent and symmetric, then (22) is conservative and at least k-th order accurate. If we further assume that $\mathbf{f}^*(\mathbf{u}_j, \mathbf{u}_l)$ is entropy conservative, then (22) is also locally entropy conservative within a single element.

Proof. Conservation: Ignoring the source term we have,

$$\begin{aligned}
\frac{d}{dt} \left(\sum_{j=0}^k \frac{\Delta x}{2} \omega_j \mathbf{u}_j \right) &= \sum_{j=0}^k \tau_j (\mathbf{f}_j - \hat{\mathbf{f}}_j) - 2 \sum_{j=0}^k \sum_{l=0}^k S_{jl} \mathbf{f}^*(\mathbf{u}_j, \mathbf{u}_l) \\
&= \sum_{j=0}^k \tau_j (\mathbf{f}_j - \hat{\mathbf{f}}_j) - \sum_{j=0}^k \sum_{l=0}^k (S_{jl} + S_{lj}) \mathbf{f}^*(\mathbf{u}_j, \mathbf{u}_l) \\
&= \sum_{j=0}^k \tau_j (\mathbf{f}_j - \hat{\mathbf{f}}_j) - \sum_{j=0}^k \sum_{l=0}^k B_{jl} \mathbf{f}^*(\mathbf{u}_j, \mathbf{u}_l), \quad (S + S^T = B) \\
&= -(\mathbf{f}_{i+1/2}^* - \mathbf{f}_{i-1/2}^*).
\end{aligned}$$

The above expression shows that the scheme is conservative within an element.

Accuracy: The accuracy analysis is easier to see in scalar case. Also, it can be easily extended for the systems case. Let $f^*(x, y) = f^*(u(x), u(y))$ and $f(x) = f(u(x))$. Then,

$$\frac{\partial f}{\partial x}(x) = \frac{\partial f^*}{\partial x}(x, x) + \frac{\partial f^*}{\partial y}(x, x) = 2 \frac{\partial f^*}{\partial y}(x, x).$$

Since the matrix D is exact for polynomials of degree up to k ,

$$\begin{aligned}
\frac{4}{\Delta x} \sum_{l=0}^k D_{jl} f^*(x(\xi_j), x(\xi_l)) &= 2 \frac{\partial f^*}{\partial y}(x(\xi_j), x(\xi_j)) + O(\Delta x^k) \\
&= \frac{\partial f}{\partial x}(x(\xi_j)) + O(\Delta x^k).
\end{aligned}$$

Entropy conservation: Entropy production within an single element can be calculated as,

$$\begin{aligned}
\frac{d}{dt} \left(\sum_{j=0}^k \frac{\Delta x}{2} \omega_j \mathcal{U}_j \right) &= \sum_{j=0}^k \frac{\Delta x}{2} \omega_j \mathbf{v}_j^T \frac{d\mathbf{u}_j}{dt} \\
&= \sum_{j=0}^k \tau_j \mathbf{v}_j^T (\mathbf{f}_j - \hat{\mathbf{f}}_j) - 2 \sum_{j=0}^k \sum_{l=0}^k S_{jl} \mathbf{v}_j^T \mathbf{f}^*(\mathbf{u}_j, \mathbf{u}_l) + \sum_{j=0}^k \frac{\Delta x}{2} \omega_j \mathbf{v}_j^T (\mathbf{s}_x)_j \\
&= \sum_{j=0}^k \tau_j \mathbf{v}_j^T (\mathbf{f}_j - \hat{\mathbf{f}}_j) - \sum_{j=0}^k \sum_{l=0}^k (B_{jl} + S_{jl} - S_{lj}) \mathbf{v}_j^T \mathbf{f}^*(\mathbf{u}_j, \mathbf{u}_l) \\
&\quad \text{(We have used } S + S^T = B \text{ and } \mathbf{v}^T \mathbf{s}_x = 0.) \quad (23) \\
&= - \sum_{j=0}^k \tau_j \mathbf{v}_j^T \hat{\mathbf{f}}_j - \sum_{j=0}^k \sum_{l=0}^k S_{jl} (\mathbf{v}_j - \mathbf{v}_l)^T \mathbf{f}^*(\mathbf{u}_j, \mathbf{u}_l) \\
&= - \sum_{j=0}^k \tau_j \mathbf{v}_j^T \hat{\mathbf{f}}_j - \sum_{j=0}^k \sum_{l=0}^k S_{jl} (\psi_j - \psi_l) \\
&= - \sum_{j=0}^k \tau_j \mathbf{v}_j^T \hat{\mathbf{f}}_j + \sum_{j=0}^k \tau_j \psi_j, \quad \text{(We have used (15).)} \\
&= (\psi_k - \mathbf{v}_k^T \hat{\mathbf{f}}_{i+1/2}) - (\psi_0 - \mathbf{v}_0^T \hat{\mathbf{f}}_{i-1/2}). \quad (24)
\end{aligned}$$

Equation (23) shows that the scheme is entropy conservative within a single element. \square

Theorem 3.2. *If the numerical flux $\hat{\mathbf{f}}$ at the element interface is entropy stable, then the scheme (22) is entropy stable.*

Proof. The entropy production rate at the interface is

$$\begin{aligned} & (\psi_k^i - (\mathbf{v}_k^i)^T \hat{\mathbf{f}}(\mathbf{u}_k^i, \mathbf{u}_0^{i+1}) - (\psi_0^{i+1} - (\mathbf{v}_0^{i+1})^T \hat{\mathbf{f}}(\mathbf{u}_k^i, \mathbf{u}_0^{i+1})) \\ & = (\mathbf{v}_0^{i+1} - \mathbf{v}_k^i)^T \hat{\mathbf{f}}(\mathbf{u}_k^i, \mathbf{u}_0^{i+1}) - (\psi_0^{i+1} - \psi_k^i). \end{aligned} \quad (25)$$

Expression (25) clearly shows that if $\hat{\mathbf{f}}$ is entropy stable then together with the compact (or periodic) boundary condition the scheme is globally entropy stable. \square

4 Entropy Stable DG Schemes: Two dimensional scheme

In this section, we will describe the two dimensional schemes. We use the rectangular mesh $I_{i,j} = [x_{i-\frac{1}{2}}, x_{i+\frac{1}{2}}] \times [y_{j-\frac{1}{2}}, y_{j+\frac{1}{2}}]$ ($1 \leq i \leq N_x$), ($1 \leq j \leq N_y$) with mesh size Δx_i and Δy_j in x and y direction, respectively. For simplicity, we consider the same number of Gauss-Lobatto points ($k+1$) in the both directions. We use the following change of variables,

$$\begin{aligned} x_i(\xi) &= \frac{1}{2}(x_{i-1/2} + x_{i+1/2}) + \frac{\xi}{2}\Delta x_i, \\ y_j(\xi) &= \frac{1}{2}(y_{j-1/2} + y_{j+1/2}) + \frac{\xi}{2}\Delta y_j. \end{aligned}$$

We denote the nodal values as, $\mathbf{u}^{p,q} = \mathbf{w}_h(x_i(\xi_p), y_j(\xi_q))$. Then for a single element $I_{i,j}$, the scheme is given by,

$$\begin{aligned} \frac{d\mathbf{u}^{p,q}}{dt} &= -\frac{2}{\Delta x} \left(\sum_{l=0}^k 2D_{pl} \mathbf{f}^*(\mathbf{u}^p, \mathbf{u}^l) - \frac{\tau_p}{\omega_p} (\mathbf{f}^{p,q} - \hat{\mathbf{f}}^{p,q}) \right) \\ &\quad - \frac{2}{\Delta y} \left(\sum_{l=0}^k 2D_{ql} \mathbf{g}^*(\mathbf{u}^q, \mathbf{u}^l) - \frac{\tau_q}{\omega_q} (\mathbf{g}^{p,q} - \hat{\mathbf{g}}^{p,q}) \right) + \mathbf{s}_x^{p,q} + \mathbf{s}_y^{p,q}, \quad (p, q = 0, 1, \dots, k) \end{aligned} \quad (26)$$

where we have used the following notations by dropping the indices i and j ,

$$\begin{aligned} [\hat{\mathbf{f}}^{0,q}, \hat{\mathbf{f}}^{1,q}, \dots, \hat{\mathbf{f}}^{k,q}] &= [\hat{\mathbf{f}}_{i-1/2,q}, 0, \dots, 0, \hat{\mathbf{f}}_{i+1/2,q}], \\ [\hat{\mathbf{g}}^{p,0}, \hat{\mathbf{g}}^{p,1}, \dots, \hat{\mathbf{g}}^{p,k}] &= [\hat{\mathbf{g}}_{p,j-1/2}, 0, \dots, 0, \hat{\mathbf{g}}_{p,j+1/2}], \\ \hat{\mathbf{f}}_{i+1/2,q} &= \hat{\mathbf{f}} \left(\mathbf{w}_h(x_{i+1/2}^-, y_j(\xi_q)), \mathbf{w}_h(x_{i+1/2}^+, y_j(\xi_q)) \right), \\ \hat{\mathbf{g}}_{p,j+1/2} &= \hat{\mathbf{g}} \left(\mathbf{w}_h(x_i(\xi_p), y_{j+1/2}^-), \mathbf{w}_h(x_i(\xi_p), y_{j+1/2}^+) \right). \end{aligned}$$

Here \mathbf{f}^* and \mathbf{g}^* are entropy conservative fluxes and the interface fluxes $\hat{\mathbf{f}}$ and $\hat{\mathbf{g}}$ are entropy stable. The proof of consistency, accuracy and entropy stability is similar to the one dimensional case (see [8]).

5 Numerical results

For the numerical test cases, we consider the cases with $k=1$, which results in a second-order scheme denoted by ESDG-O2 and $k=2$, which results in a third-order scheme ESDG-O3. For the time integration, we use SSP Runge-Kutta ([18]) second and third-order time discretization for ESDG-O2 and ESDG-O3 schemes, respectively. We make following choices to complete the description of the scheme:

- **Entropy conservative flux:** We use the entropy conservative fluxes \mathbf{f}^* and \mathbf{g}^* presented in [31], and described in Appendix A.
- **Entropy stable flux:** For the entropy stable fluxes $\hat{\mathbf{f}}$, and $\hat{\mathbf{g}}$, we use Lax-Friedrich numerical fluxes.

For one-dimensional problems, we use the TVDM limiter [9] in order to avoid the spurious oscillations. The TVDM limiter uses $M = 10$ unless stated explicitly. Note that, use of such a limiter at the post-processing does not guaranty the entropy stability. We also use the bound preserving limiter presented in [26], wherever needed. Bound preserving limiter does not increase the entropy (see [8]). We use CFL 0.2 for all test cases, where CFL condition is implemented following [8].

5.1 One dimensional numerical tests

We will now present the results for the one dimensional test cases.

Test Problem 1. Accuracy test (without source): In this test problem, we demonstrate the formal order of accuracy of the schemes without the source terms. Ignoring the source terms by taking $W = 0$, we consider the following exact solution $[-0.5, 0.5]$,

$$\rho(x, t) = 2 + \sin(2\pi(x - t)), v^x(x, 0) = 1, v^y(x, 0) = 0, p^{xx}(x, 0) = p^{yy}(x, 0) = 1, p^{xy}(x, 0) = 0.$$

A periodic boundary is used for the computations. Error is computed using the exact solution at $T = 0.5$.

We present the L^1 and L^∞ errors and order of accuracy for the density in Tables1 using the ESDG-O2

N	L^1 error	Order	L^∞ error	Order
32	2.58e-02	...	2.34e-02	...
64	6.50e-03	1.99	5.61e-03	2.06
128	1.63e-03	2.00	1.39e-03	2.02
256	4.07e-04	2.00	3.45e-04	2.00
512	1.02e-04	2.00	8.63e-05	2.00

Table 1: L^1 and L^∞ errors and order of accuracy for density using ESDG-O2

N	L^1 error	Order	L^∞ error	Order
32	6.27e-04	...	5.64e-04	...
64	8.34e-05	2.91	7.46e-05	2.92
128	1.06e-05	2.97	9.40e-06	2.99
256	1.34e-06	2.99	1.17e-06	3.00
512	1.67e-07	3.00	1.46e-07	3.00

Table 2: L^1 and L^∞ errors and order of accuracy for density using ESDG-O3

scheme. We observe that the schemes have reached the desired second order of accuracy. Similarly, in Table 2, we have presented errors for ESDG-O3. Here again, we observe that the proposed scheme has a third-order accuracy.

Test Problem 2. Accuracy test (with source): In this test problem, we check the order of accuracy of the schemes by considering a time dependent source corresponds to the potential, $W = \sin(2\pi(x - t))$. We consider the following smooth exact solution in domain $x \in [-0.5, 0.5]$ for this test case:

$$\rho(x, t) = 2 + \sin(2\pi(x - t)), v^x(x, 0) = 1, v^y(x, 0) = 0,$$

$$p^{xx}(x, t) = 1.5 + \frac{1}{8} (\cos(4\pi(x - t)) - 8 \sin(2\pi(x - t))), p^{xy}(x, 0) = 0, p^{yy}(x, 0) = 1.$$

N	L^1 error	Order	L^∞ error	Order
32	9.48e-02	...	1.71e-01	...
64	2.50e-02	1.93	4.76e-02	1.84
128	6.32e-03	1.98	1.31e-02	1.86
256	1.58e-03	2.00	3.41e-03	1.95
512	3.96e-04	2.00	8.62e-04	1.98

Table 3: Accuracy table of ESDG-O2

N	L^1 error	Order	L^∞ error	Order
32	1.51e-03	...	2.45e-03	...
64	2.30e-04	2.71	4.05e-04	2.59
128	3.17e-05	2.86	5.07e-05	3.00
256	4.23e-06	2.91	5.91e-06	3.10
512	5.83e-07	2.86	1.00e-06	2.56

Table 4: Accuracy table of ESDG-O3

We present the results at $T = 0.5$ using periodic boundary. The errors and order of accuracy for density are presented in Table 3 and 4 for ESDG-O2 and ESDG-O3 schemes, respectively. In both cases, we observe that the schemes have the desired order of accuracy.

Test Problem 3. Sod shock tube Riemann problem: We consider the Riemann problem on the domain $n \in [-0.5, 0.5]$ with initial discontinuity at $x = 0$. The left and right states are given in Table 5. We use outflow boundary conditions, and the solutions are presented at time of $T = 0.125$. The exact solution of the problem contains a shock, contact wave, and rarefaction wave. We do not need bound preserving limiter for this test case. TVBM limiter was used to control the oscillations. The numerical solutions are

States	ρ	v^x	v^y	p^{xx}	p^{xy}	p^{yy}
Left	1	0	0	2	0.05	0.6
Right	0.125	0	0	0.2	0.1	0.2

Table 5: Test Problem 3: Initial conditions for Sod shock tube problem

presented in Figure 1, using 100 and 500 cells for ESDG-O2($k=1$) and ESDG-O3($k=2$) schemes. We have plotted density, velocity and the pressure components. We observe that both schemes are able to resolve all the waves and as expected ESDG-O3 is more accurate than the ESDG-O2 scheme. Furthermore, the use of finer grids $N = 500$ significantly improves the results. We also note that the results are comparable with [26, 31].

We have also plotted the time evolution of total entropy. We note that at 500, entropy decay is lower than at the 100 cells. Furthermore, both ESDG-O2 and ESDG-O3 having similar decay, with ESDG-O2 having slightly lower decay at 100 cells when compared to ESDG-O3. However, at 500 cells, ESDG-O3 having lower entropy decay than the ESDG-O2.

Test Problem 4. Two shock waves This is another Riemann problem (see[26, 27, 1]) where the exact solution contains two shock waves moving away from each other. We consider the domain $[-0.5, 0.5]$ with outflow boundary conditions. The initial discontinuity is centered at $x = 0$ separating the left and right states given in Table 6. Bound preserving limiter is not required for this test. Computational results are plotted at final time $T = 0.125$. Numerical results are plotted in Figure 2 for ESDG-O2($k=1$) and ESDG-O3($k=2$) at resolutions of 100 and 500 cells. We have again plotted density, velocity and pressure

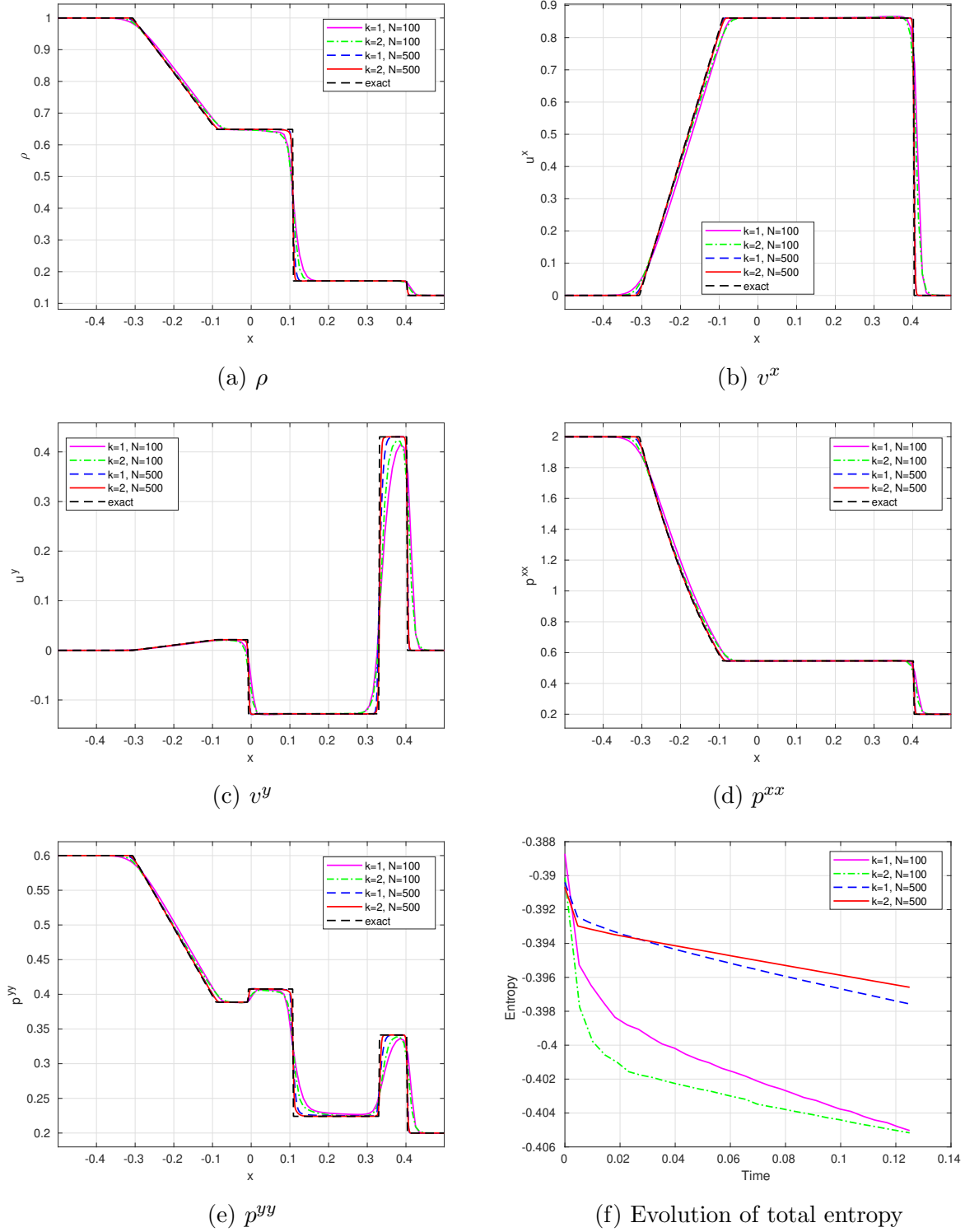


Figure 1: Test Problem 3 (Sod shock tube problem): Plot of density, velocity, pressure components and total entropy evolution for ESDG-O2($k=1$) and ESDG-O3($k=2$) using 100 and 500 cells.

components. We note that both the schemes are able to capture the shocks and results improve significantly when we use finer mesh of 500 cells. In addition, ESDG-O3 is more accurate than the ESDG-O2. Also, results are comparable to those presented in [26, 27].

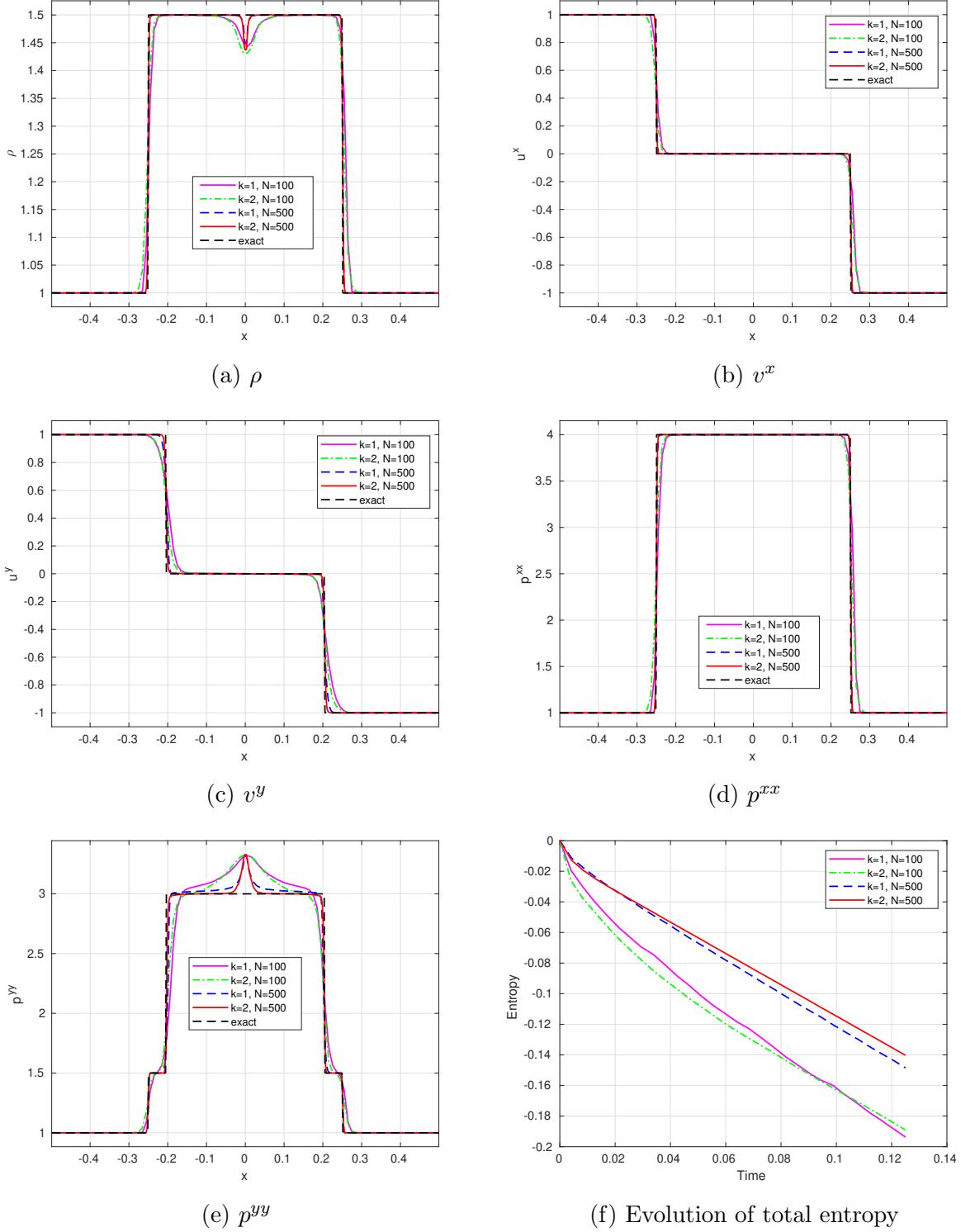


Figure 2: Test Problem 4 (Two shock waves): Plot of density, velocity, pressure components and total entropy evolution for ESDG-O2($k=1$) and ESDG-O3($k=2$) using 100 and 500 cells.

From the total entropy decay plot, we observe that entropy decay decreases significantly when the resolution is increased from 100 to 500 cells. Furthermore, entropy decay of the ESDG-O3 scheme is lower than the ESDG-O2 scheme.

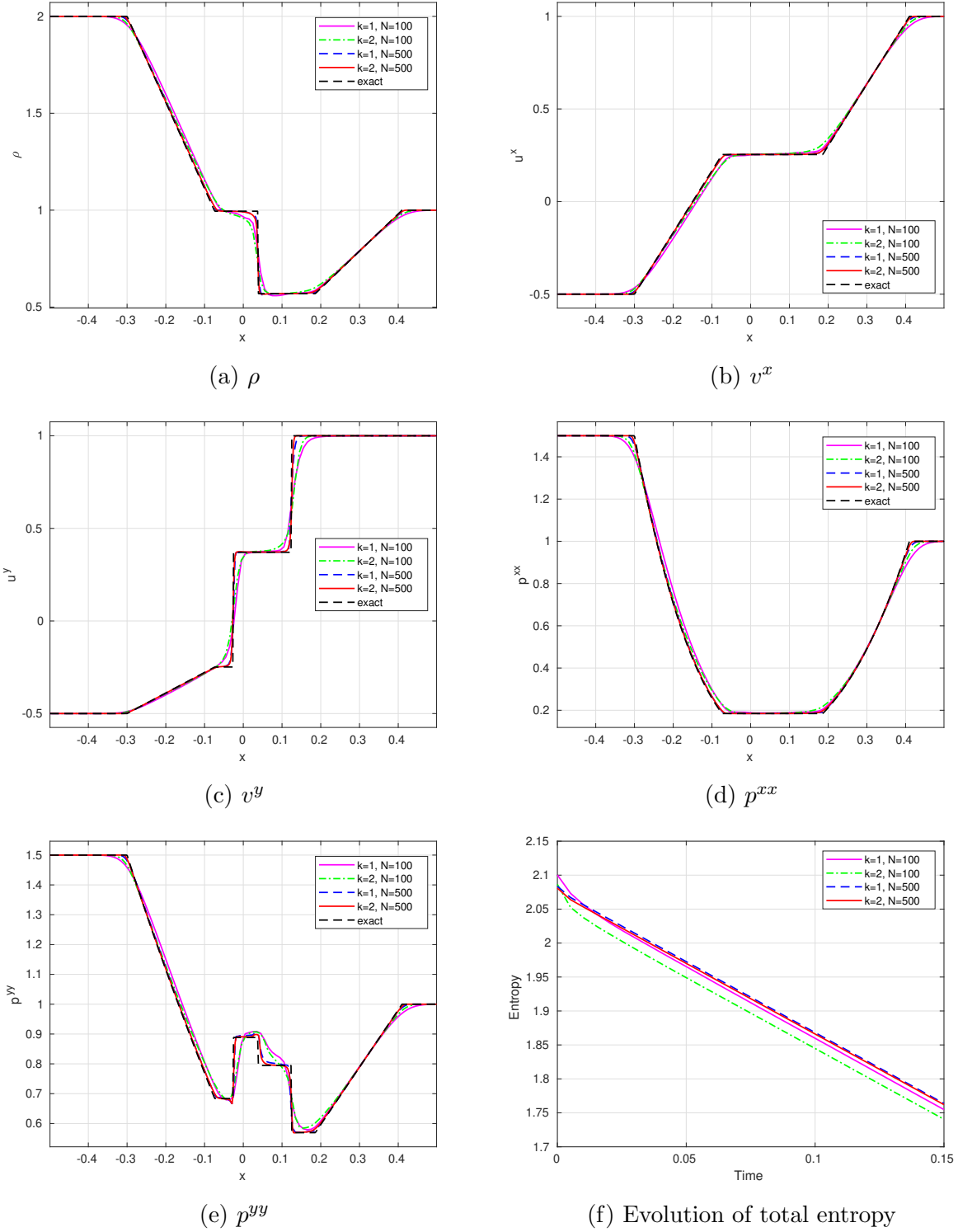


Figure 3: Test Problem 5 (Two rarefaction waves): Plot of density, velocity, pressure components and total entropy evolution for ESDG-O2($k=1$) and ESDG-O3($k=2$) using 100 and 500 cells.

Test Problem 5. Two rarefaction waves In this test case, we consider a Riemann problem, where the exact solution contains two rarefaction waves. The test case is set in the domain $[-0.5, 0.5]$ with the initial jump at $x = 0$ is separating two states given in Table 7. Similar to the last two cases, we use outflow boundary conditions. The solutions are computed until time $T = 0.15$ using 100 and 500 cells.

States	ρ	v^x	v^y	p^{xx}	p^{xy}	p^{yy}
Left	1	1	1	1	0	1
Right	1	-1	-1	1	0	1

Table 6: Test Problem 4: Initial conditions for the two shock waves problem

States	ρ	v^x	v^y	p^{xx}	p^{xy}	p^{yy}
Left	2	-0.5	-0.5	1.5	0.5	1.5
Right	1	1	1	1	0	1

Table 7: Test Problem 5: Initial conditions for two rarefaction waves problem

The numerical solutions are presented in Figure 3 for both schemes. We observe the similar performance of the schemes as in the last two test cases, with ESDG-O3 more accurate than the ESDG-O2 scheme. Furthermore, both of the schemes are able to capture all the waves. In addition, numerical results are consistent with results in [1, 26, 27]. We also note from the total entropy decay plot that the schemes have similar entropy decay.

Test Problem 6. Near vacuum state This test case is designed to test robustness of the schemes at low density and pressure (see [26, 27]). The domain $[-0.5, 0.5]$ consists of left and right states, given in Table 7, separated at $x = 0$. We have simulated the solution till time $T = 0.05$ using outflow boundary conditions. Even though we have low density and pressure areas, we have not used bound preserving limiter.

States	ρ	v^x	v^y	p^{xx}	p^{xy}	p^{yy}
Left	1	-5	0	2	0	2
Right	1	5	0	2	0	2

Table 8: Test Problem 6: Initial conditions for the near vacuum state problem

Numerical results are plotted in Figure 4 for both schemes. We observe that both the schemes are able to capture two outgoing rarefaction waves, and both are stable. Also, at the finer resolution of 500 cells, the results are highly accurate and comparable to those presented in [26, 27].

Test Problem 7. Two rarefaction waves problem with Gaussian source This is another test case, where we test the robustness of the scheme in low density and pressure areas. However, in this case the low density and pressure areas are generated via source terms. We consider the computational domain of $[0, 4]$ with outflow boundary conditions and the initial discontinuity is placed at $x = 2$. The left and right states are given in Table 9. To test the effects of source terms, following [26, 27], we consider the Gaussian source term corresponding to

$$W(x, t) = 25 \exp(-200(x - 2)^2).$$

Computational results for both schemes are plotted in Figure 5 at $T = 0.1$. In this test, we use bound preserving limiter for both the schemes. We again observe that both of these schemes are able to capture all the features of the solution, and both are stable. Furthermore, the solution is highly accurate at the finer mesh of 500 cells.

Test Problem 8. Shu-Osher test problem This test problem is obtained by modifying the Shu-Osher test case problem for Euler equations ([32, 27]). We consider the computational domain of $[-5, 5]$

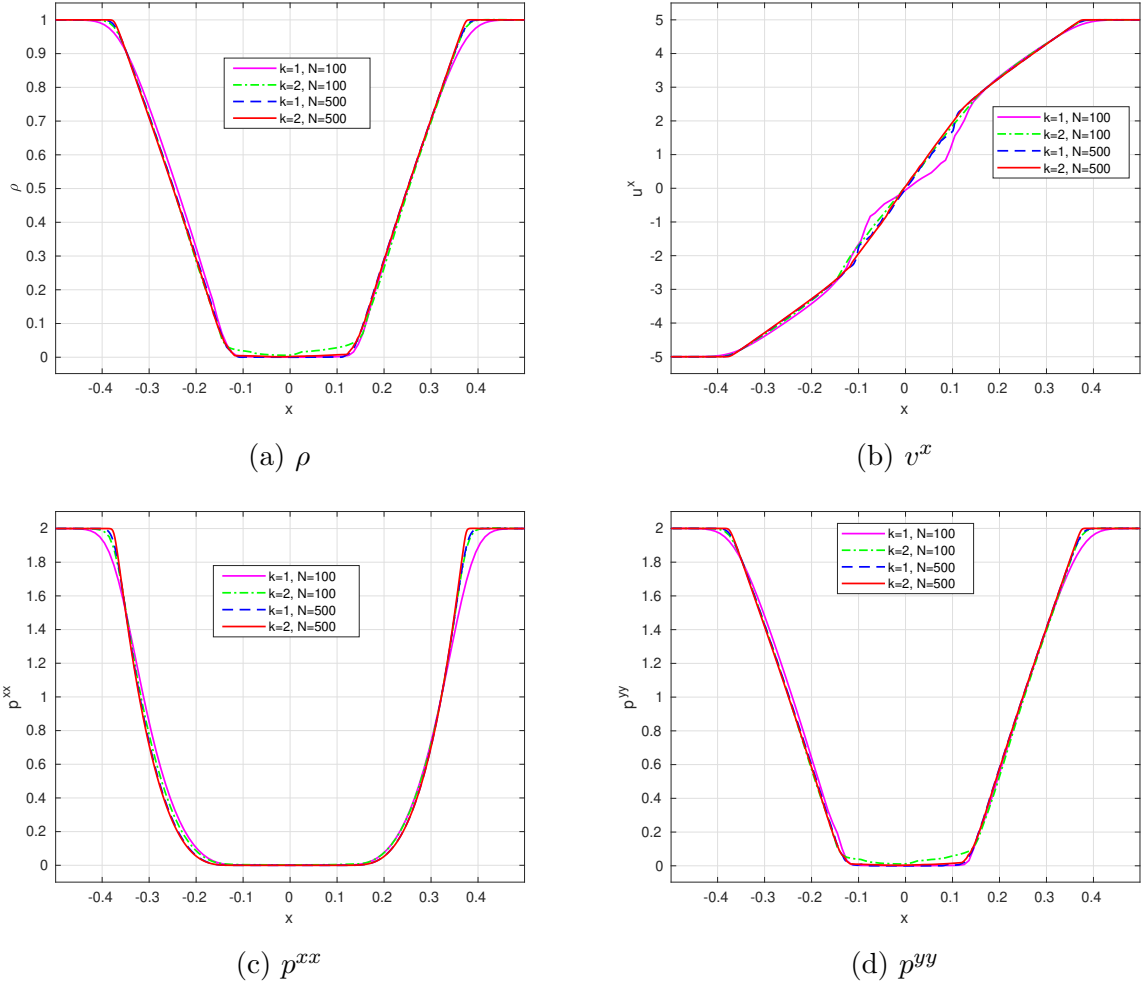


Figure 4: Test Problem 6 (Near vacuum state): Plot of density, velocity and pressure components for ESDG-O2($k=1$) and ESDG-O3($k=2$) using 100 and 500 cells.

States	ρ	v^x	v^y	p^{xx}	p^{xy}	p^{yy}
Left	1	-4	0	9	7	9
Right	1	4	0	9	7	9

Table 9: Test Problem 7: Initial conditions for two rarefaction waves with Gaussian source term problem

with initial discontinuity at $x = -4$, which separates states given in Table 10. The computations are performed using 200 and 500 cells till time $T = 1.8$. Results show that both ESDG-O2 and ESDG-O3 schemes are capable of resolving the small-scale features of the flow. We note that the results using the fine grid ($N = 500$) are much more accurate than the results on the coarse grid ($N = 200$).

5.2 Two dimensional numerical tests

We will now present two dimensional test cases.

Test Problem 9. Two dimensional near vacuum test problem In this test case from [26, 27], we have a low density and low-pressure zone, hence we will test the robustness of the algorithms. We

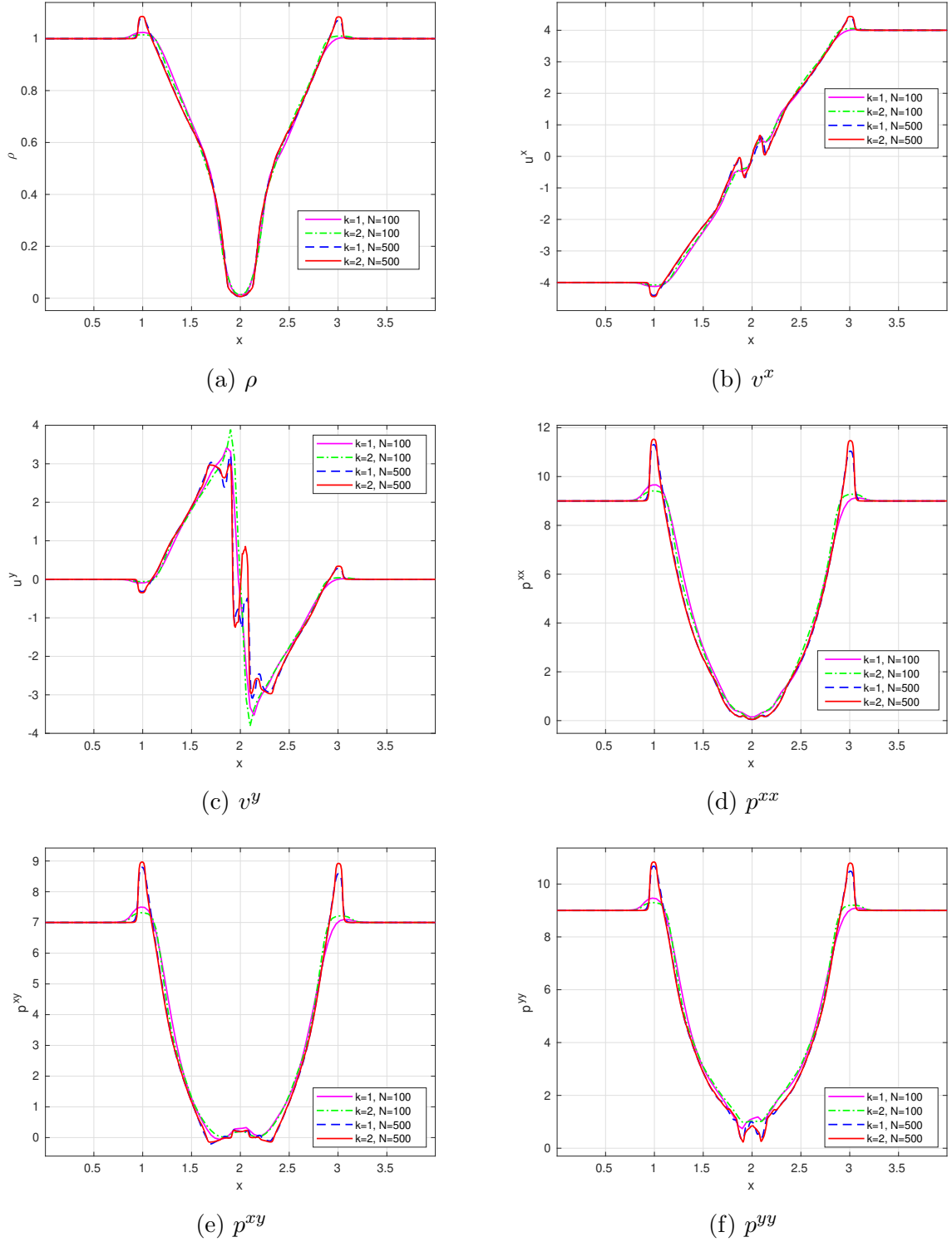


Figure 5: Test Problem 7 (Two rarefaction waves problem with Gaussian source): Plot of density, velocity and pressure components for ESDG-O2 and ESDG-O3 using 100 and 500 cells.

consider the computational domain $[-2, 2] \times [-2, 2]$ with outflow boundary conditions. Density is taken to be unity throughout the domain, whereas the pressure components are, $p^{xx} = p^{yy} = 2, p^{xy} = 0$. The velocity is set to be $8(x/r, y/r)$, where $r = \sqrt{x^2 + y^2}$. Simulations are performed using 100×100 mesh until $T = 0.05$. Bound preserving limiter is used during the simulations. The numerical results for

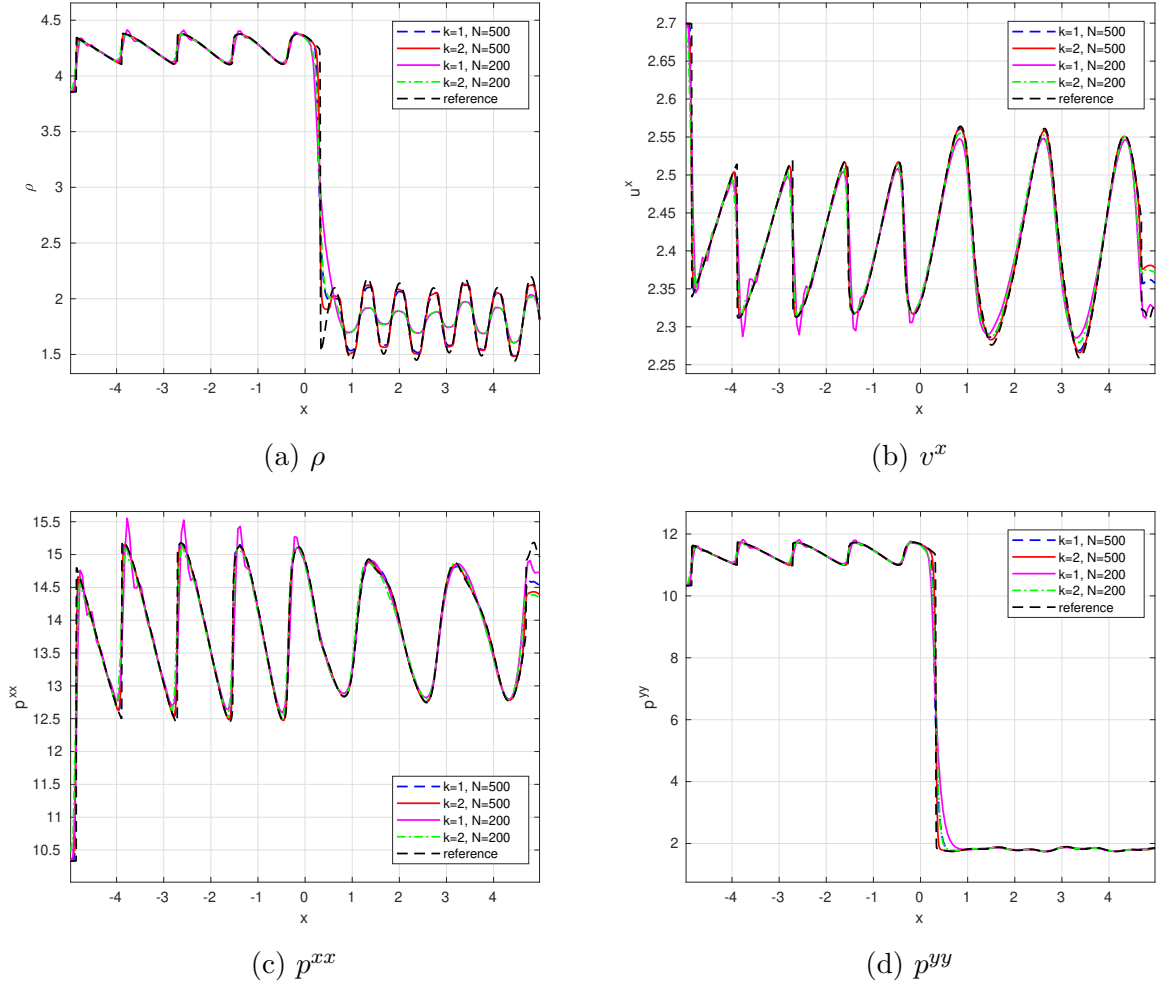


Figure 6: Test Problem 8 (Shu-Osher test problem): Plot of density, velocity and pressure components for ESDG-O2($k=1$) and ESDG-O3($k=2$) using 100 and 500 cells.

ESDG-O2 are presented in Figure 7, and for ESDG-O3, they are presented in Figure 8. Both schemes are able to resolve the solutions with similar details and give results consistent with [27].

Test Problem 10. Uniform plasma state with Gaussian source We consider another test case from [26, 27]. The computational domain $[0, 4] \times [0, 4]$ is assumed to contain uniform initial state,

$$\rho = 0.1, v^x = v^y = 0.0, p^{xx} = p^{yy} = 9.0, p^{xy} = 7.0.$$

The source terms are used using a Gaussian profile given by,

$$W(x, y, t) = 25 \exp(-200((x-2)^2 + (y-2)^2)).$$

We compute the solution using 100×100 mesh, until $T = 0.1$. Bound preserving limiter is not used here. Numerical results are plotted in Figure 9a, and 9b shows an an-isotropic change in the density due to

States	ρ	v^x	v^y	p^{xx}	p^{xy}	p^{yy}
Left	3.857143	2.699369	0	10.33333	0	10.33333
Right	$1 + 0.2 \sin(5x)$	0	0	1	0	1

Table 10: Test Problem 8: Initial conditions for Shu-Osher test problem

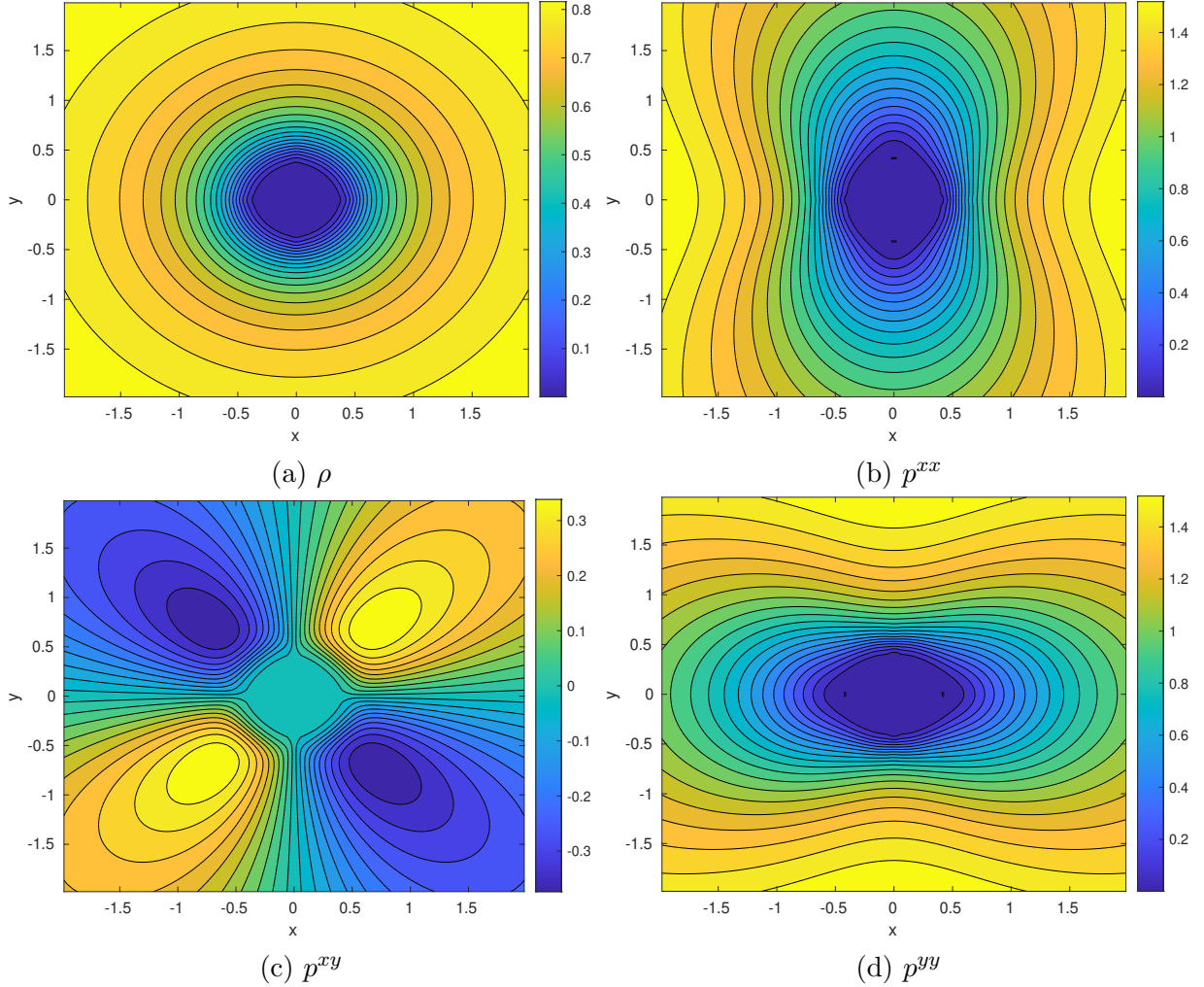


Figure 7: Test Problem 9 (Two dimensional near vacuum test problem): Plot of density and pressure components for ESDG-O2 at time $t = 0.05$ using 100×100 mesh.

the source. Figure 9c shows the one dimensional cut of the results along $x + y = 4$. We note that both ESDG-O2 and ESDG-O3 have similar performance.

Test Problem 11. Realistic simulation in two dimensions In this test problem from [2], we consider the domain $[0, 100] \times [0, 100]$ filled with initial state,

$$\rho = 0.109885, v^x = v^y = 0.0, p^{xx} = p^{yy} = 1.0, p^{xy} = 0.0.$$

We then consider a Gaussian source corresponds to

$$W(x, y, t) = \exp\left(-\left(\frac{x-50}{10}\right)^2 - \left(\frac{y-50}{10}\right)^2\right),$$

only in x -direction i.e. source in y -direction is set to be zero. Furthermore, an additional source $2v_T\rho W$ ($v_T \in [0, 1]$) is added to the energy equations (see [2, 26]). We present the solutions with $v_T = 0$ and $v_T = 1$ at $T = 0.5$. Figure 10 and Figure 11 show the results by ESDG-O2 and ESDG-O3 schemes, respectively. We clearly observe that both schemes have similar performance at this resolution and obtained results are consistent with the results in [26]. One dimensional cut of the solution along the diagonal $x + y = 4$ in Figure 9c and Figure 10c shows that the computed density is lower when $v_T = 1$.

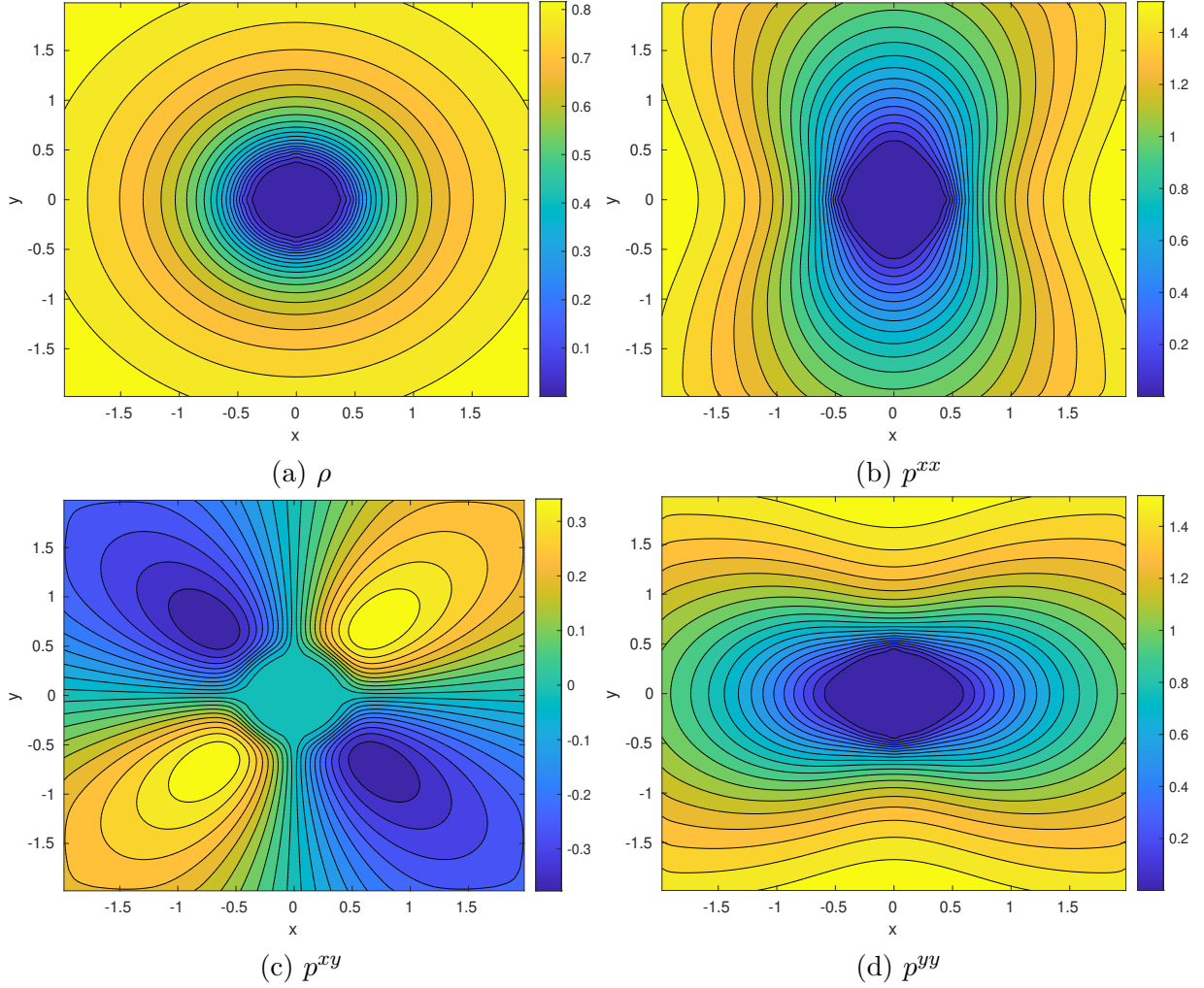


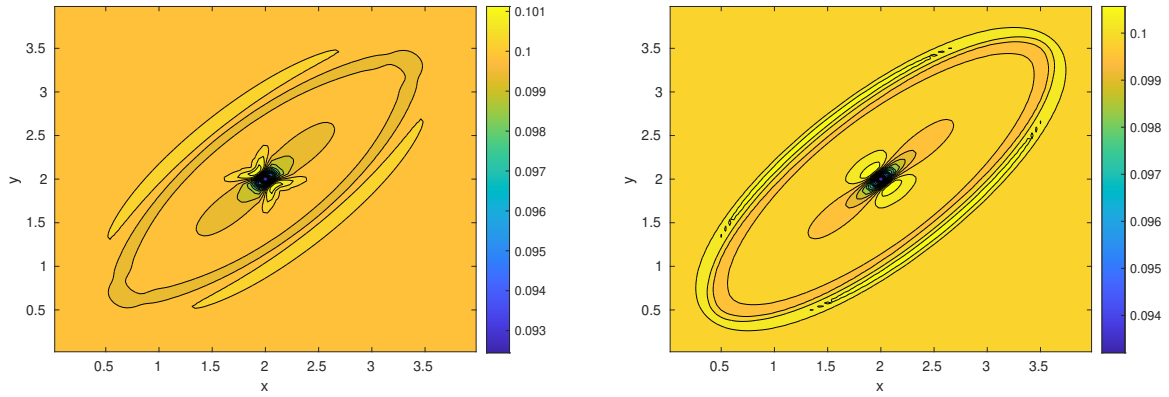
Figure 8: Test Problem 9 (Two dimensional near vacuum test problem): Plot of density and pressure components for ESDG-O3 at time $t = 0.05$ using 100×100 mesh.

Conclusion

In this article, we have considered the ten-moment equations. We first present the entropy framework for the system. We then design the entropy stable discontinuous Galerkin scheme for the system in one and two dimensions. To achieve the entropy stability; we use entropy conservative numerical flux in cells and entropy stable numerical flux at the cell interfaces. This is achieved by following the quadrature rules in [8]. The resulting schemes are shown to be entropy stable at the semi-discrete level, with source terms. For the time discretization, we have used SSP Runge Kutta methods. These schemes are then tested on a variety of test cases in one and two dimensions. Furthermore, schemes are demonstrated to be accurate in capturing various waves and entropy stable, in both one and two dimensions.

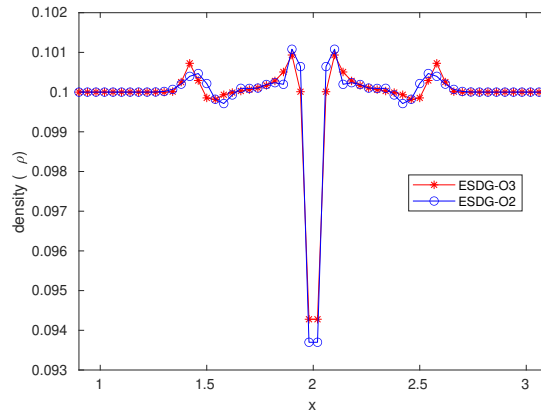
Acknowledgment

Harish Kumar has been funded in part by SERB, DST MATRICS grant with file No. MTR/2019/000380.



(a) ESDG-O2

(b) ESDG-O3

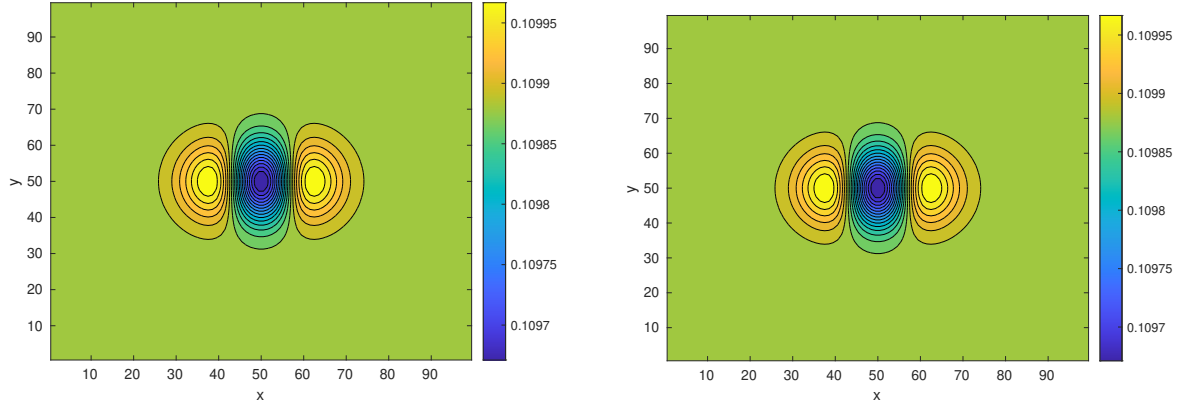


(c) One dimensional cut of the computed solution (density) along the diagonal $x+y=4$.

Figure 9: Test Problem 10 (Uniform plasma state with Gaussian source): Plot of density using ESDG-O2 and ESDG-O3 schemes at time $t = 0.1$ on 100×100 mesh.

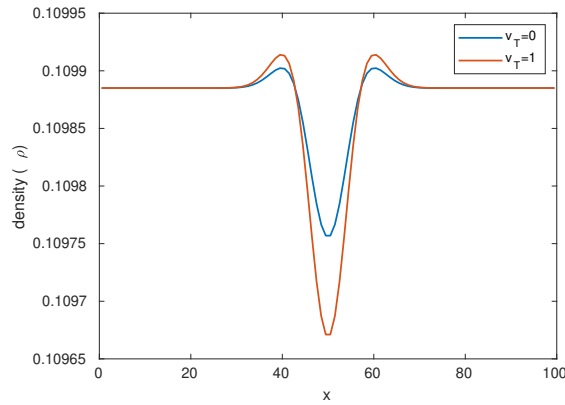
References

- [1] BERTHON, C. Numerical approximations of the 10-moment Gaussian closure. *Mathematics of Computation* 75, 256 (2006), 1809–1831.
- [2] BERTHON, C., DUBROCA, B., AND SANGAM, A. An entropy preserving relaxation scheme for ten-moments equations with source terms. *Communications in Mathematical Sciences* 13, 8 (2015), 2119–2154.
- [3] BISWAS, B., AND DUBEY, R. K. Low dissipative entropy stable schemes using third order WENO and TVD reconstructions. *Advances in Computational Mathematics* 44, 4 (2018), 1153–1181.
- [4] BISWAS, B., AND KUMAR, H. Entropy stable discontinuous Galerkin approximation for the Relativistic Hydrodynamic Equations. *arXiv preprint arXiv:1911.07488* (2019).
- [5] BROWN, S., ROE, P., AND GROTH, C. Numerical solution of a 10-moment model for nonequilibrium gasdynamics. In *12th Computational Fluid Dynamics Conference*. American Institute of Aeronautics and Astronautics.



(a) $v_T = 0$

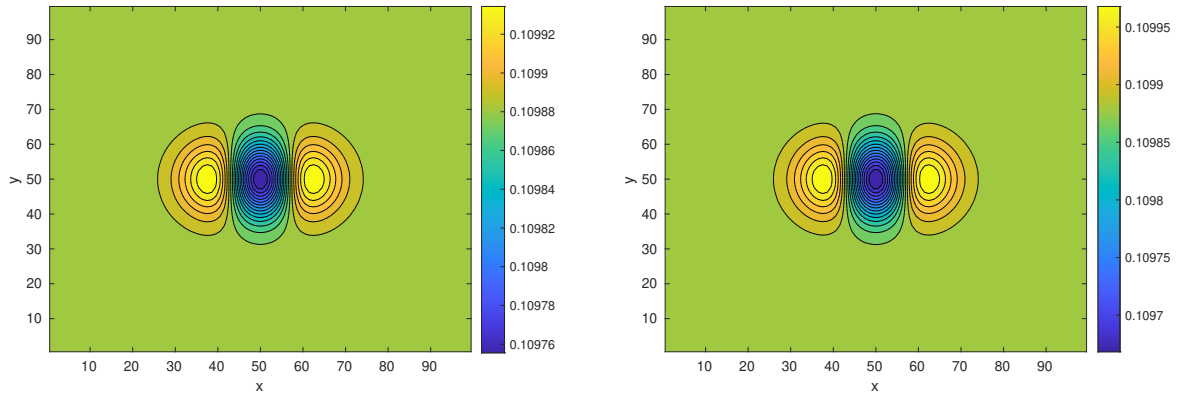
(b) $v_T = 1$



(c) One dimensional cut of the computed solution (density) along the diagonal $x+y=4$.

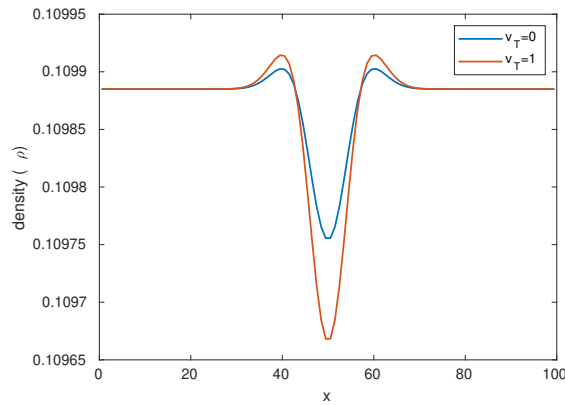
Figure 10: Test Problem 11 (Realistic simulation in two dimensions): Plot of density approximated using ESDG-O2 scheme at time $t = 0.5$ with 100×100 mesh.

- [6] CARPENTER, M. H., FISHER, T. C., NIELSEN, E. J., AND FRANKEL, S. H. Entropy Stable Spectral Collocation Schemes for the Navier–Stokes Equations: Discontinuous Interfaces. *SIAM Journal on Scientific Computing* 36, 5 (2014), B835–B867.
- [7] CHAVENT, G., AND COCKBURN, B. The local projection $P^0 - P^1$ -discontinuous-Galerkin finite element method for scalar conservation laws. *ESAIM: Mathematical Modelling and Numerical Analysis* 23, 4 (1989), 565–592.
- [8] CHEN, T., AND SHU, C.-W. Entropy stable high order discontinuous Galerkin methods with suitable quadrature rules for hyperbolic conservation laws. *Journal of Computational Physics* 345 (2017), 427–461.
- [9] COCKBURN, B. Discontinuous Galerkin Methods for Convection-Dominated Problems. *Journal of scientific computing* 16, 3 (1999), 69–224.
- [10] COCKBURN, B., AND SHU, C.-W. TVB Runge-Kutta local projection discontinuous Galerkin finite element method for conservation laws. II. General framework. *Mathematics of Computation* 52, 186 (1989), 411–411.



(a) $v_T = 0$

(b) $v_T = 1$



(c) One dimensional cut of the computed solution (density) along the diagonal $x+y=4$.

Figure 11: Test Problem 11 (Realistic simulation in two dimensions): Plot of density approximated using ESDG-O3 scheme at time $t = 0.5$ with 100×100 mesh.

- [11] COCKBURN, B., AND SHU, C.-W. The Runge-Kutta local projection P^1 -discontinuous-Galerkin finite element method for scalar conservation laws. *ESAIM: Mathematical Modelling and Numerical Analysis* 25, 3 (1991), 337–361.
- [12] DUAN, J., AND TANG, H. High-order accurate entropy stable nodal discontinuous Galerkin schemes for the ideal special relativistic magnetohydrodynamics. *arXiv preprint arXiv:1911.03825* (2019).
- [13] DUBEY, R. K., AND BISWAS, B. Suitable diffusion for constructing non-oscillatory entropy stable schemes. *Journal of Computational Physics* 372 (2018), 912–930.
- [14] DUBROCA, B., TCHONG, M., CHARRIER, P., TIKHONCHUK, V. T., AND MORREEUW, J.-P. Magnetic field generation in plasmas due to anisotropic laser heating. *Physics of Plasmas* 11, 8 (July 2004), 3830–3839.
- [15] FJORDHOLM, U. S., MISHRA, S., AND TADMOR, E. Arbitrarily High-order Accurate Entropy Stable Essentially Nonoscillatory Schemes for Systems of Conservation Laws. *SIAM Journal on Numerical Analysis* 50, 2 (2012), 544–573.
- [16] FJORDHOLM, U. S., AND RAY, D. A Sign Preserving WENO Reconstruction Method. *Journal of Scientific Computing* 68, 1 (2016), 42–63.

- [17] GASSNER, G. J., WINTERS, A. R., AND KOPRIVA, D. A. A well balanced and entropy conservative discontinuous Galerkin spectral element method for the shallow water equations. *Applied Mathematics and Computation* 272 (2016), 291–308.
- [18] GOTTLIEB, S., SHU, C.-W., AND TADMOR, E. Strong Stability-Preserving High-Order Time Discretization Methods. *SIAM Review* 43, 1 (2001), 89–112.
- [19] HIRABAYASHI, K., HOSHINO, M., AND AMANO, T. A new framework for magnetohydrodynamic simulations with anisotropic pressure. *Journal of Computational Physics* 327 (Dec. 2016), 851–872.
- [20] LEVEQUE, R. J. *Numerical Methods for Conservation Laws*, 2 ed. Lectures in Mathematics. ETH Zürich. Birkhäuser Basel, Basel, 1992.
- [21] LEVERMORE, C. D. Moment closure hierarchies for kinetic theories. *Journal of Statistical Physics* 83, 5-6 (1996), 1021–1065.
- [22] LEVERMORE, C. D., AND MOROKOFF, W. J. The Gaussian Moment Closure for Gas Dynamics. *SIAM Journal on Applied Mathematics* 59, 1 (1998), 72–96.
- [23] LIU, Y., SHU, C.-W., AND ZHANG, M. Entropy stable high order discontinuous Galerkin methods for ideal compressible MHD on structured meshes. *Journal of Computational Physics* 354 (2018), 163–178.
- [24] MEENA, A. K., AND KUMAR, H. A well-balanced scheme for Ten-Moment Gaussian closure equations with source term. *Zeitschrift für angewandte Mathematik und Physik* 69, 1 (2018), 8.
- [25] MEENA, A. K., AND KUMAR, H. Robust numerical schemes for Two-Fluid Ten-Moment plasma flow equations. *Zeitschrift für angewandte Mathematik und Physik* 70, 1 (Feb. 2019), 23.
- [26] MEENA, A. K., KUMAR, H., AND CHANDRASHEKAR, P. Positivity-preserving high-order discontinuous Galerkin schemes for Ten-Moment Gaussian closure equations. *Journal of Computational Physics* 339 (2017), 370–395.
- [27] MEENA, A. K., KUMAR, R., AND CHANDRASHEKAR, P. Positivity-Preserving Finite Difference WENO Scheme for Ten-Moment Equations with Source Term. *Journal of Scientific Computing* 82, 1 (2020), 15.
- [28] MENG, X., TTH, G., SOKOLOV, I. V., AND GOMBOSI, T. I. Classical and semirelativistic magnetohydrodynamics with anisotropic ion pressure. *Journal of Computational Physics* 231, 9 (May 2012), 3610–3622.
- [29] MILLER, S. T., AND SHUMLAK, U. A multi-species 13-moment model for moderately collisional plasmas. *Physics of Plasmas* 23, 8 (Aug. 2016), 082303.
- [30] REED, W. H., AND HILL, T. R. Triangular Mesh Methods for the Neutron Transport Equation. Tech. rep., Los Alamos Scientific Lab., N. Mex.(USA), 1973.
- [31] SEN, C., AND KUMAR, H. Entropy Stable Schemes For Ten-Moment Gaussian Closure Equations. *Journal of Scientific Computing* 75, 2 (2018), 1128–1155.
- [32] SHU, C.-W., AND OSHER, S. Efficient implementation of essentially non-oscillatory shock-capturing schemes. *Journal of Computational Physics* 77, 2 (1988), 439–471.

Appendix A Entropy conservative flux

We denote,

$$D = \frac{\det(\mathbf{p})}{\rho}, \beta_{xx} = \frac{p^{xx}}{D}, \beta_{xy} = \frac{p^{xy}}{D}, \beta_{yy} = \frac{p^{yy}}{D}, D_\beta = \beta_{xx}\beta_{yy} - \beta_{xy}^2.$$

Then the entropy conservative fluxes $\mathbf{f}^* = [f_1^*, f_2^*, f_3^*, f_4^*, f_5^*, f_6^*]^T$ and $\mathbf{g}^* = [g_1^*, g_2^*, g_3^*, g_4^*, g_5^*, g_6^*]^T$ are given by (see [31].),

$$\mathbf{f}^* = \begin{pmatrix} \rho^{ln} \bar{v}^x \\ f_1^* \bar{v}^x + \frac{\bar{\rho} \bar{\beta}_{xx}}{\bar{\beta}_{xx} \bar{\beta}_{yy} - (\bar{\beta}_{xy})^2} \\ f_1^* \bar{v}^y + \frac{\bar{\rho} \bar{\beta}_{xy}}{\bar{\beta}_{xx} \bar{\beta}_{yy} - (\bar{\beta}_{xy})^2} \\ \left(\frac{\bar{\beta}_{xx}}{D_\beta^{ln}} - \overline{(v^x)^2} \right) f_1^* + 2\bar{v}^x f_2^* \\ \left(\frac{\bar{\beta}_{xy}}{D_\beta^{ln}} - \overline{v^x v^y} \right) f_1^* + \bar{v}^x f_3^* + \bar{v}^y f_2^* \\ \left(\frac{\bar{\beta}_{yy}}{D_\beta^{ln}} - \overline{(v^y)^2} \right) f_1^* + 2\bar{v}^y f_3^* \end{pmatrix}$$

$$\mathbf{g}^* = \begin{pmatrix} \rho^{ln} \bar{v}^y \\ g_1^* \bar{v}^x + \frac{\bar{\rho} \bar{\beta}_{xy}}{\bar{\beta}_{xx} \bar{\beta}_{yy} - (\bar{\beta}_{xy})^2} \\ g_1^* \bar{v}^y + \frac{\bar{\rho} \bar{\beta}_{yy}}{\bar{\beta}_{xx} \bar{\beta}_{yy} - (\bar{\beta}_{xy})^2} \\ \left(\frac{\bar{\beta}_{xx}}{D_\beta^{ln}} - \overline{(v^x)^2} \right) g_1^* + 2\bar{v}^x g_2^* \\ \left(\frac{\bar{\beta}_{xy}}{D_\beta^{ln}} - \overline{v^x v^y} \right) g_1^* + \bar{v}^x g_3^* + \bar{v}^y g_2^* \\ \left(\frac{\bar{\beta}_{yy}}{D_\beta^{ln}} - \overline{(v^y)^2} \right) g_1^* + 2\bar{v}^y g_3^* \end{pmatrix}$$